J. Iron Steel Res. Int.
https://doi.org/10.1007/s42243-021-00588-0

ORIGINAL PAPER

Effect of copper on edge cracking behavior and microstructure of rolled austenitic stainless steel plate

Guang-hui Zhao[1,2] · Jian Zhang[1,2] · Juan Li[1,2] · Hua-ying Li[1,2] · Hai-tao Liu[3] · Li-feng Ma[1,2]

Received: 9 November 2020 / Revised: 3 March 2021 / Accepted: 5 March 2021

Abstract
Cu is known to affect the edge cracking characteristics of austenitic stainless steel as it causes embrittlement. The hot rolling test of four kinds of austenitic stainless steel with different copper content (0, 2.42, 3.60 and 4.35 wt.%) was carried out to examine the effect of hot rolling cracks on steel containing different copper contents. The evolution of crack and microstructure was analyzed using the scanning electron microscope, energy-dispersive spectrometer, electron back scattered diffraction and transmission electron microscope. Experimental results showed an upward trend in edge cracking degree when Cu content was 4.35%, and the crack extended from the edge of the steel plate to the middle by about 14 mm. Besides, severe oxidation was observed inside the crack by fractography. With the increase in copper content at 1250 °C, the content of {110}<112> brass and {112}<111> copper textures decreased. When the content of copper was 4.35%, the decrease was most significant, and {112}<111> copper texture content decreased to only 0.5%. Generally, the textures of 2.42%Cu and 3.60%Cu 304L steel changed little, while a large change in the texture of 4.35%Cu 304L steel was observed. To conclude, the increase in rolling temperature can prevent edge crack and its propagation effectively.

Keywords Austenitic stainless steel · Copper · Edge crack · Microstructure · Ferrite

1 Introduction

Antibacterial austenitic stainless steel is widely used in home decoration, food and medical industries due to its excellent high temperature performance [1, 2]. Adding an appropriate amount of copper to steel leads to nano-particle precipitation, thus significantly improving the strength, corrosion resistance, cold workability, and antibacterial properties of steel [3–5]. Especially, Li [6] and Xi et al. [7] have shown that steel containing 0.5%–4.0% copper has better antibacterial properties than traditional stainless steel after heat treatment.

✉ Jian Zhang
zj2926298864@163.com

[1] School of Mechanical Engineering, Taiyuan University of Science and Technology, Taiyuan 030024, Shanxi, China

[2] Shanxi Provincial Key Laboratory of Metallurgical Device Design Theory and Technology, Taiyuan 030024, Shanxi, China

[3] State Key Laboratory of Rolling and Automation, Northeastern University, Shenyang 110819, Liaoning, China

However, excessive copper elements in the rolled products bring about copper brittleness and edge cracks in rolling, greatly limiting the application of copper-containing steel in the industry. In the heating process before rolling, the defect area on the surface of the oxidized slab will decarburize the structure near the crack and generate a large number of secondary oxide particles [8]. It is noted that copper with a lower melting point flows along the grain boundaries at high temperatures, and forms low temperature eutectic phases that preferentially segregate to the grain boundaries, leading to grain boundary embrittlement in steel [9].

Cracks often appear on both sides of the copper-containing steel coil, or on the surface of the steel plate in the form of pockmarks. The macro morphology of copper embrittlement is similar to cracks or pitted microcrack defects caused by overburning [10]. Therefore, an assessment in the effect of copper on the edge cracking characteristics of austenitic stainless steel during rolling is essential. In the present study, the evolution of the copper-containing austenitic stainless steel as well as its edge morphology, microstructure and texture was investigated.

Published online: 29 May 2021

Meanwhile, the influence of copper on hot rolling deformation of austenitic stainless steel was studied, and the scheme of austenitic stainless steel cracks with different copper contents was given, which provided a basis for further research on the development of the novel antibacterial stainless steel.

2 Materials and methods

2.1 Materials

The ingot was made of electroslag remelting casting produced by Taiyuan Iron and Steel Group Co., Ltd., and its composition is shown in Table 1.

2.2 Experiment method

The copper-containing cast-rolled austenitic stainless steel with the initial size of 100 mm × 70 mm × 30 mm (length, width and thickness, respectively) was rolled by the two-high rolling mill with the total reduction of roller maintained at 80% and the rolling speed at 0.2 m/s (Fig. 1a) after the cast-rolled sheets were pre-heated at 1150 and 1250 °C, separately. The sheets were subjected to 8 passes, with the interval of 8 s. Air cooling was carried out after final rolling.

The microstructures of edge cracks on the transversal sections of rolling direction (RD)–transverse direction (TD) and the RD–normal direction (ND) planes (i.e., sampling locations 1 and 2 respectively in Fig. 1b, respectively) were characterized using a ZEISS scanning electron microscope (SEM), and the precipitated phase was analyzed using an energy-dispersive spectrometer (EDS). The copper-containing austenitic stainless steel samples were prepared by the standard metallographic method, and 10% oxalic acid was used for electrolytic corrosion. The microtexture and edge cracks on the RD–TD plane of the plates were monitored by the electron back scattered diffraction (EBSD) method. The EBSD samples were prepared by electrochemical polishing with mixed solution of 10 vol.% perchloric acid + 90 vol.% alcohol at a current of 0.8 A for 90 s. Finally, post-processing software (Channel 5) was used for data analysis. Transmission electron microscope (TEM) samples were cut from the RD–TD section of the hot rolling specimens, ground to 100 μm thick, and subjected to ion milling. Then, the samples were analyzed by JEOL F200 TEM. In addition, cracks with different shapes were produced in the longitudinal section of RD–TD after heating. The largest crack appeared almost every 100 mm in the TD direction. Therefore, the edge cracks of the four types of steel plates after rolling were analyzed with the macroscopic observation method as the evaluation standard.

3 Results

3.1 Microstructure before and after rolling

Figure 2 illustrates the microstructures of austenitic stainless steel with different copper contents in the radial direction of the ingot. The cast stainless steel consists of coarse and dendritic austenite columnar structure and a few spot or vermicular second phase structures distributing at the grain boundaries. It could be observed from Fig. 2a–c that the dendrites in the ingot gradually became larger as the copper content increased, and gradually changed from one direction distribution to discontinuous distribution in the matrix. The direction of 4.35%Cu 304L dendrites tended to be axial, and the secondary dendrites were arranged in parallel. The formation of the special microstructure might be due to a large degree of subcooling at the edge of the ingot. It is well known that nickel has an expanding austenite phase region and chromium is a ferrite stabilizing element. As shown in the EDS surface scan (Fig. 1f), position 1 in Fig. 1e is bright due to the high temperature ferrite content, and position 2 is the austenite matrix because of the high Ni content. The copper element is easily solved in the austenite, and the color in position 1 is dim. The copper element fluctuation at the phase boundary of position 3 shown in the EDS line scan indicates that the copper element was segregated here, and the copper content in the austenite matrix was higher than that in the ferrite.

Table 1 Chemical composition of austenitic stainless steel (wt.%)

Steel	C	Si	Mn	P	S	Cr	Ni	Cu	Fe
304L	0.005	0.42	1.51	0.004	0.001	17.88	8.80	0	71.38
2.42%Cu 304L	0.007	0.42	1.53	0.010	0.001	18.29	8.70	2.42	68.62
3.60%Cu 304L	0.007	0.49	1.54	0.013	0.001	17.91	8.72	3.60	67.72
4.35%Cu 304L	0.008	0.52	1.48	0.010	0.001	17.90	8.81	4.35	66.92

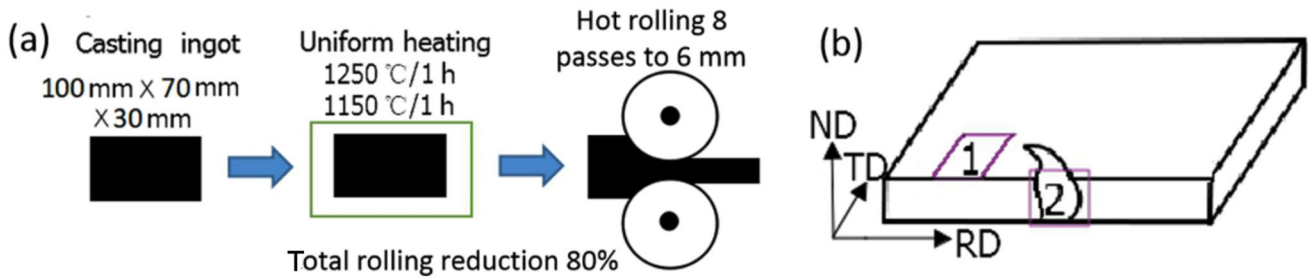

Fig. 1 Rolling process and sampling position of copper-containing rolled steel

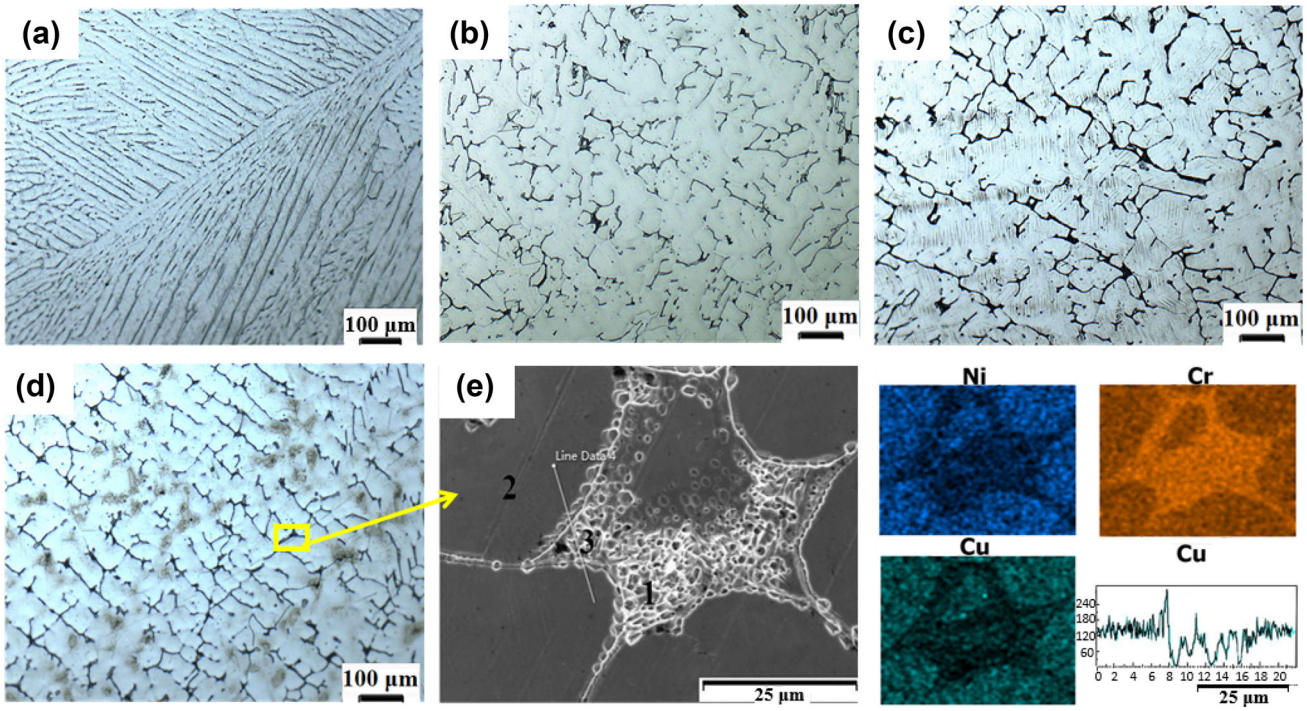

Fig. 2 As-cast metallographic structure of austenitic stainless steel with different copper contents. **a** 304L steel; **b** 2.42%Cu 304L steel; **c** 3.60%Cu 304L steel; **d** 4.35%Cu 304L steel; **e** SEM photos of as-cast 4.35%Cu 304L steel; **f** EDS photos of as-cast 4.35%Cu 304L steel (Line Data 4 represents element line scan of EDS)

The microstructures of plates at different pre-rolling temperatures can be observed in the inverse pole figure (IPF), phase maps and kernel average misorientation (KAM) of copper-containing austenitic stainless steel samples as shown in Figs. 3 and 4. Ingots eliminated voids, dendritic structures and macro segregation in the casting during hot rolling. The initial coarse grain of RD-ND planes was elongated along the rolling direction after repeated rolling. The width of the band-shaped grains in the plate rolled at 1150 °C decreased with the increase in the copper content. The band-shaped ferrite became more and more elongated and its content decreased gradually.

However, it is shown in Fig. 4 that the grains grew wider and fine grains appeared between narrow grain boundaries when the pre-rolling temperature was 1250 °C. The recrystallized grains grew bigger along the grain boundary and were distributed like a necklace, which coincided with the viewpoints of Ponge and Gottstein [11], who beheld that the necklace-like grains generally produced in the early discontinuous dynamic recrystallization process.

The addition of copper reduced the stacking fault energy and increased the critical deformation of dynamic recrystallization, which made it difficult for austenitic stainless steel to deform. At the same time, the precipitates dispersed in the microstructure pinned dislocations or grain boundaries, which hindered the continuous dynamic recrystallization process (Table 2). The proportion of twins in the structure was small, which decreased from 0.44% to 0.39% at 1150 °C and increased from 0.39% to 0.44% at 1250 °C with the increase in copper content.

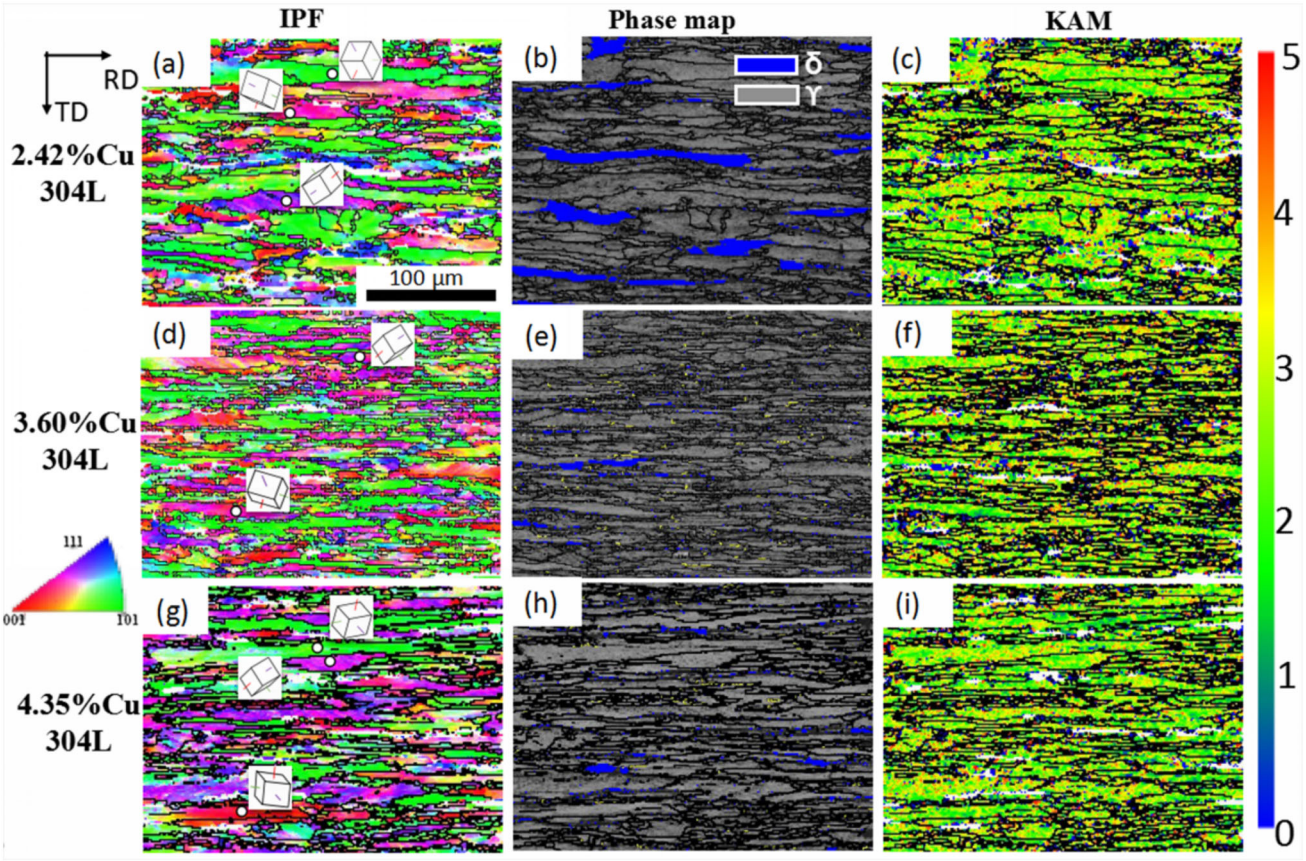

Fig. 3 IPFs, phase maps and local KAM value distribution maps of 304L stainless steel with different copper contents after rolling at 1150 °C. **a**–**c** 2.42%Cu 304L steel; **d**–**f** 3.60%Cu 304L steel; **g**–**i** 4.35%Cu 304L steel. Blue part is ferrite and yellow part is twin

According to IPF maps of different samples shown in Figs. 3a, d, g and 4a, d, g with the increase in copper content, the orientation of green <101> decreased, and red <001> changed to purple $<\bar{2}11>$. The orientation of green <101> increased with the rising temperature. The KAM maps of the samples (Figs. 3c, f, i and 4c, f, i) reflect the deformation state inside the grain. The staggered imaging method is an intuitive plastic deformation method [12]. Therefore, the higher the local KAM value, the greater the deformation degree of the grain and the larger the corresponding strain amount.

3.2 Morphology of rolling cracks

Figure 5a, b presents the macroscopic crack maps of rolled copper-containing austenitic stainless steel. A lot of cracks were distributed along the rolling direction and extended from the edge to the center of the plate. The edge crack of 304L austenitic stainless steel plate was small after rolling. With the increase in copper content at pre-rolling temperature of 1150 °C, the edge crack increased. However, the degree of edge crack decreased with the temperature increasing to 1250 °C. The crack characteristics changed from short and loose to deep and continuous. The largest edge crack existed in 4.35%Cu 304L steel at 1150 °C. It formed an angle of about 45° with the rolling direction and extended from the edge to the middle by about 14 mm. Figure 5c, d shows the relationship between the average number of macro cracks (within 100 mm), the average crack depth and the interval distance at the edge of austenitic stainless steel plates with different copper contents after hot rolling at 1150 and 1250 °C. Hot rolling cracks were more sensitive to heating temperature. With the increase in copper content at 1150 °C, the average number of cracks decreased, the average crack depth increased, and the average distance between cracks was shortened. However, the raised copper content increased the average crack number and depth at 1250 °C.

Figure 5e–h is fractography of cracks along the rolling edge of various copper-containing steels at 1150 °C. There are fine cracks at the flanks of 304L steel. It is shown in Fig. 5e that there are evident folds around the fracture surface. The cracks on the edge of steel plate got more severe when copper content increased. The widest crack of 2.42%Cu 304L steel reached 800 μm, whereas the cracks on 3.60%Cu 304L and 4.35%Cu 304L steels extended to

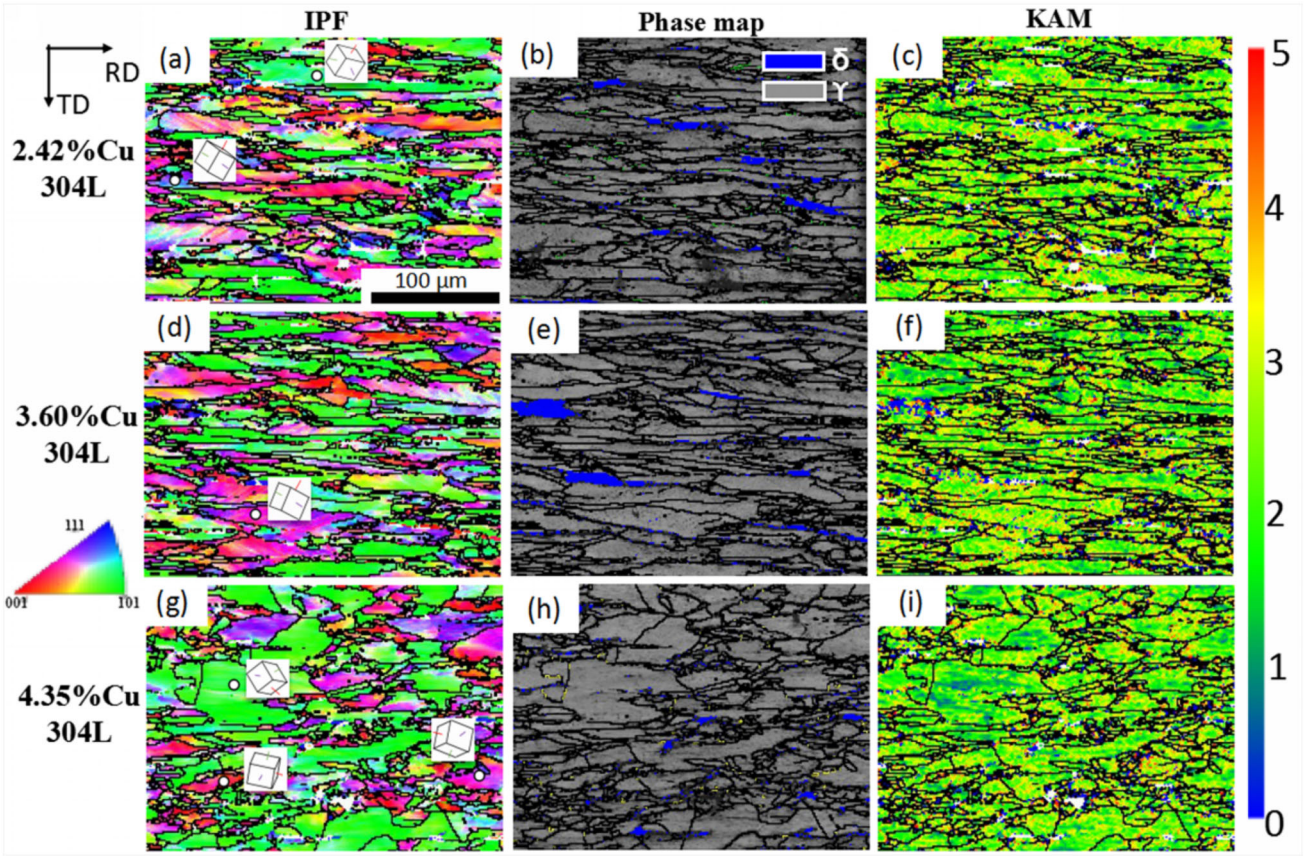

Fig. 4 IPFs, phase maps and local KAM value distribution maps of 304L stainless steel with different copper contents after rolling at 1250 °C. **a–c** 2.42%Cu 304L steel; **d–f** 3.60%Cu 304L steel; **g–i** 4.35%Cu 304L steel

Table 2 500 × area EBSD statistics for recrystallization, twinning and ferrite ratio after hot rolling at 1150 and 1250 °C (%)

EBSD statistics	Pre-rolling temperature of 1150 °C			Pre-rolling temperature of 1250 °C		
	2.42%Cu 304L steel	3.60%Cu 304L steel	4.35%Cu 304L steel	2.42%Cu 304L steel	3.60%Cu 304L steel	4.35%Cu 304L steel
Recrystallization	3.66	3.55	3.28	2.97	2.92	2.61
Twinning	0.44	0.42	0.39	0.27	0.31	0.36
Ferrite ratio	7.29	2.98	2.3	3.39	3.14	1.83

cover the entire rolled plate, demonstrating a poor forming performance.

Figure 6 shows the cracking fracture surface and composition of 4.35%Cu 304L steel at different pre-rolling temperatures. No inclusions were found in the main crack, while the extension line of the secondary crack was seriously oxidized. Cracks are further enlarged to observe the morphological characteristics. There were a large number of angular-shaped substances in the cracks at 1250 °C and the edge cracks at 1150 °C. EDS point scan results reveals a great deal of Fe, Cu, and Cr oxides around the cracks. Cu oxides were basically angular, and their content was 9.6% and 7.9% at 1150 and 1250 °C, respectively, both of which exceeded that in the matrix. As shown in the EDS scan results of the cracking fracture surface of 4.35%Cu 304L stainless steel at 1250 °C in Fig. 6, the content of Fe, Cr and O was relatively high, the copper-rich layer formed on the oxides around the crack, and the content of copper was 5.0%, which was higher than that in the matrix. The copper elements in the matrix were polymerized to form oxides with high brittleness and hardness, leading to the separation from the matrix interface, and subsequently the production of longitudinal cracks under the action of tensile stress.

The IPFs, phase maps and strain contouring shown in Figs. 7 and 8 illustrate the microstructure around the crack tip of various copper-containing steel samples. The grains

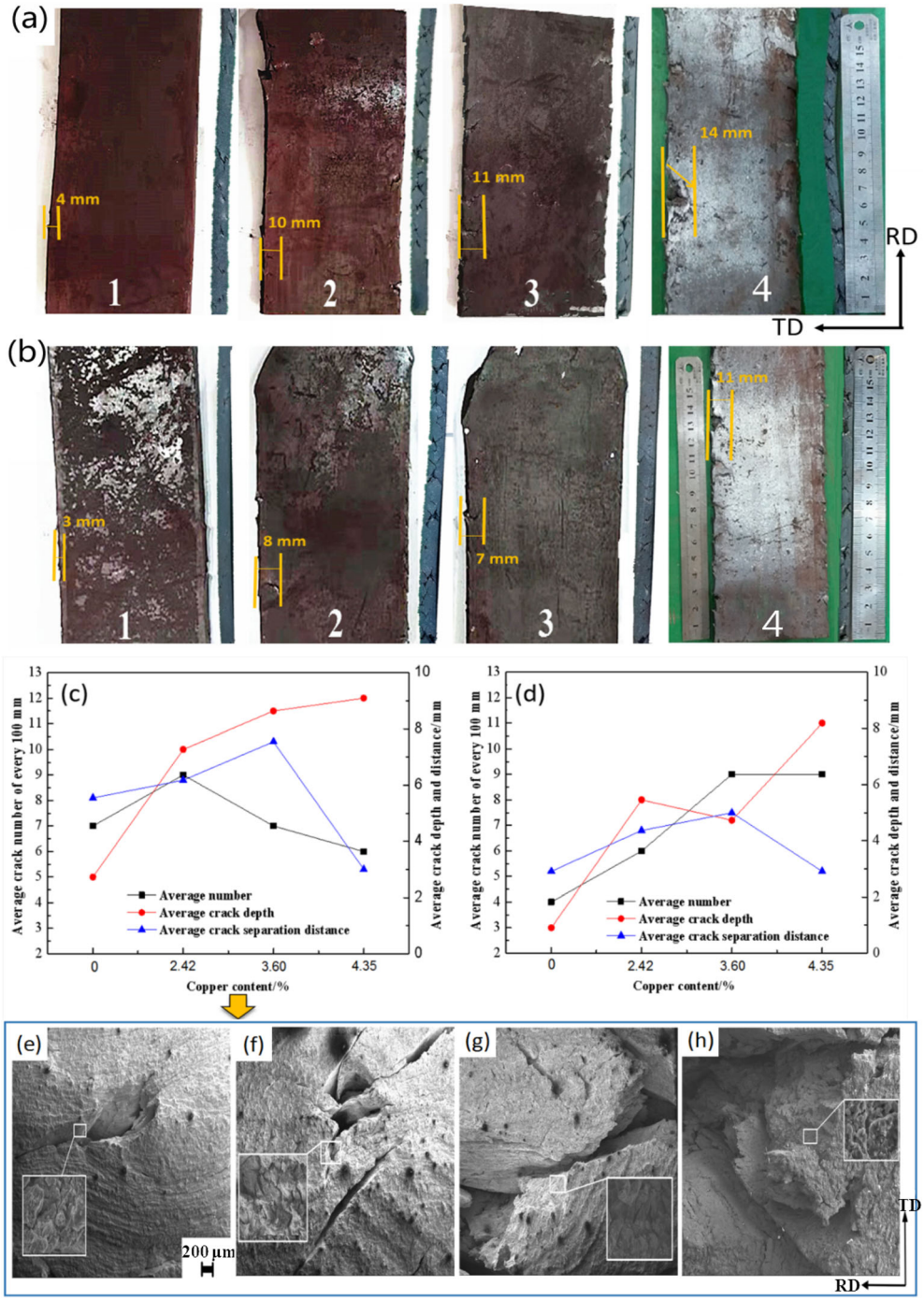

Fig. 5 Statistical maps, macroscopic cracks and fractography of hot-rolled copper-containing steel at different pre-rolling temperatures of 1150 °C (**a, c**) and 1250 °C (**b, d**) and fractography of cracks along rolling edge of 304L steel (**e**), 2.42%Cu 304L steel (**f**), 3.60%Cu 304L steel (**g**) and 4.35%Cu 304L steel (**h**) at 1150 °C. 1–304L steel; 2–2.42%Cu 304L steel; 3–3.60%Cu 304L steel; 4–4.35%Cu 304L steel

in the structure were unevenly mixed when the heating temperature was 1150 °C. Coarse grains had higher yield strength than fine grains, resulting in additional stress between the two types of grains. Yue et al. [13] found that the stress concentration between grains would lead to the production of cracks along the coarse grains. It is shown in the strain contouring maps in Figs. 7 and 8 that the blue color appeared around the crack indicated that the strain value was very small and the stress has been released. However, compared with the ferrite distribution map and strain contouring map, the red color appeared around individual ferrite, such as the arrows in Figs. 7 and 8,

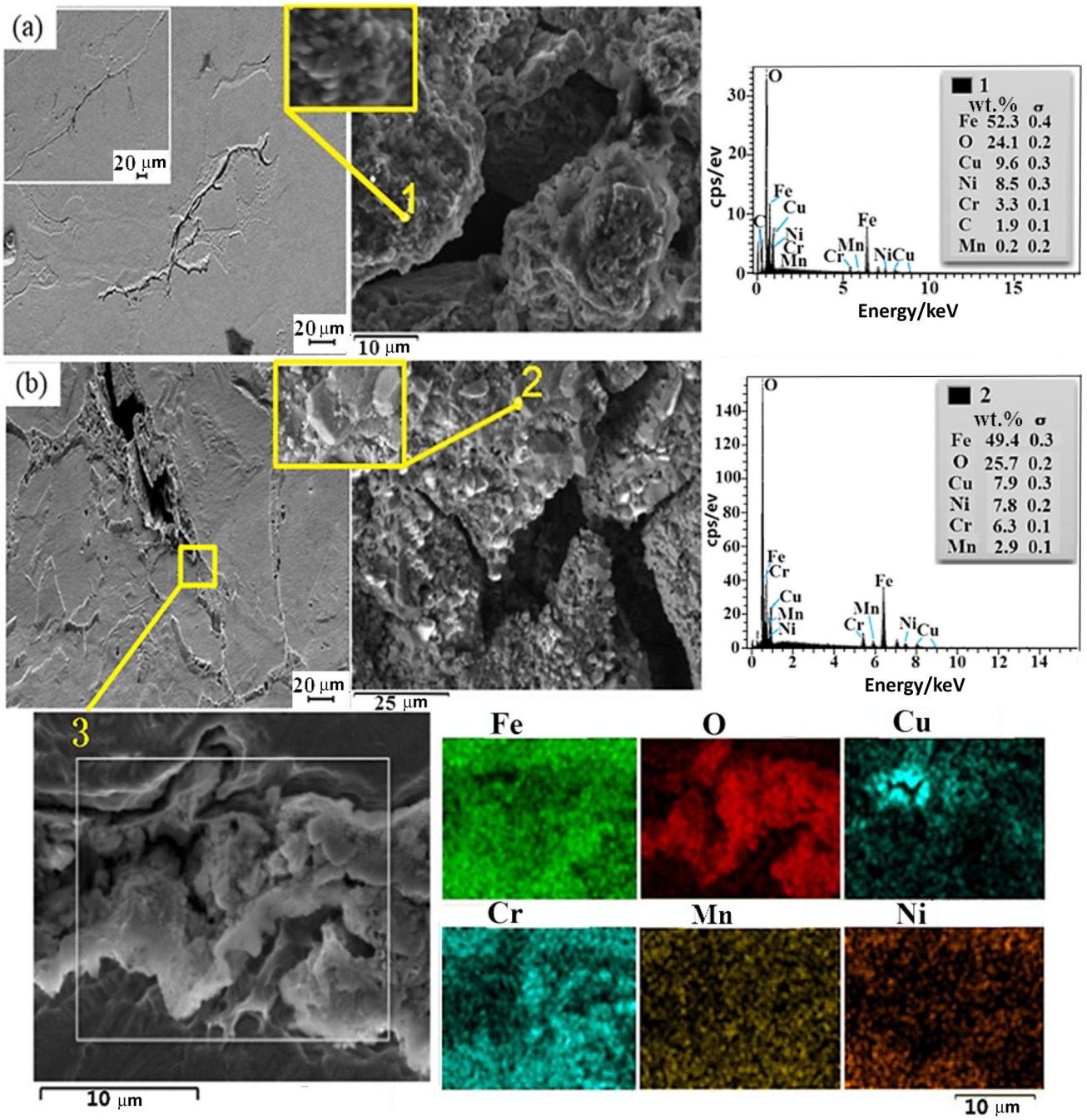

Fig. 6 Crack fracture surface and composition of 4.35%Cu 304L steel at different heating temperatures. **a** 1150 °C; **b** 1250 °C. σ Deviation of component measurement proportion

indicated that the strain value was very high. With the increase in copper content, the main crack expanded. Several secondary cracks in 4.35%Cu 304L steel were generated at the end of the main crack, and they rapidly extended to the inside of the rolled plate as indicated by the arrows in Figs. 7g and 8g. A large number of fine recrystallized grains were found around the secondary cracks. The random distribution orientation of the grains in the recrystallization zone indicated that samples had no texture or the grains had no preferred orientation (Figs. 7g and 8g). The recrystallized fine grains could effectively prevent the crack from further extending due to a large area of grain boundary. The rising temperature facilitated recrystallization [8], which effectively improved the crack-resisting performance of the plate.

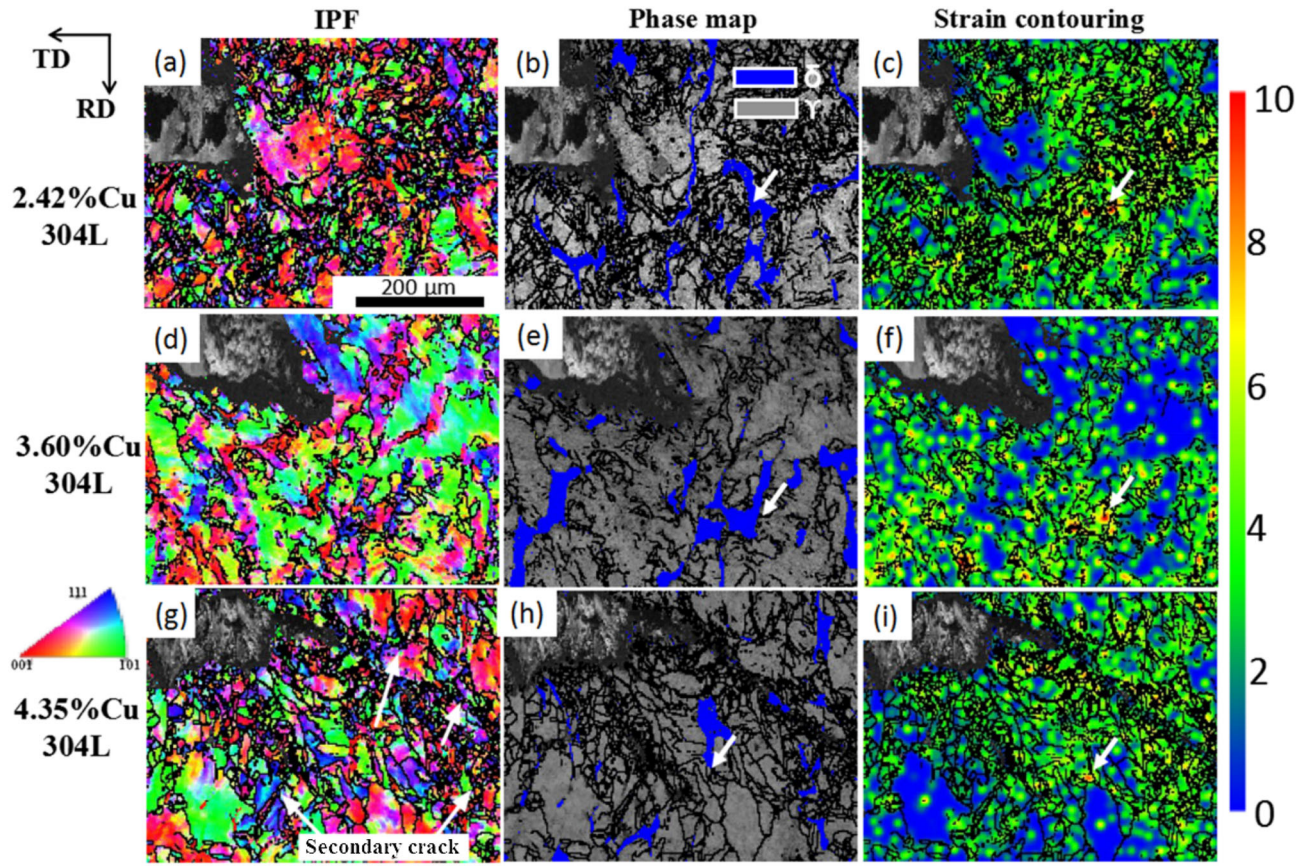

Fig. 7 IPFs, phase maps and strain contouring of microstructure around crack tip at 1150 °C. **a–c** 2.42%Cu 304L steel; **d–f** 3.60%Cu 304L steel; **g–i** 4.35%Cu 304L steel

4 Discussion

4.1 Effect of copper on ferrite in austenitic steel

The composition and morphology of ferrite are affected by the chemical properties of steel (especially Cu content) and the change in heating temperature. There was high temperature ferrite distributed on the grain boundary in the process of casting. With the increase in copper content, the morphology of ferrite in the steel gradually changed to an island shape, accompanied by copper segregation at the phase boundary between austenite and ferrite. It was observed by Suutala [14] that the ferrite morphology varied with alloy composition and solidification cooling speed, making the as-cast structure of the material more complex. It is shown in Table 3 and Fig. 9c that the Cr/Ni equivalent ratio of copper-containing austenitic stainless steel decreased gradually in this experiment, and the ferrite content of steel decreased accordingly [15, 16]. The solidification mode of austenite phase equilibrium changed from ferrite–austenite (FA, with fraction of austenite to ferite larger than 3/4) solidification mode to austenite-ferrite (AF, with fraction of ferite to austenite larger than 3/4) solidification mode. In the process of non-equilibrium crystallization, the addition of copper in the steel reduced the occurrence of composition segregation, resulting in the volume change of high-temperature ferrite.

The ferrite phase of 4.5% Cu-304L at room temperature was distributed as an island and reticular shape (Fig. 9a, b). The ferrite gradually coarsened and its proportion increased in the subsequent heating process. It has been reported that the dissolution of ferrite is related to the diffusion of Cr and Ni in the austenite [17]. During the dissolution process of ferrite in austenite, the morphology changes from long needle to short needle or even spherical, and the volume fraction of the phase decreased as the treatment temperature rose [18]. Copper was also an element to improve austenite stability simultaneously. Ferrite was difficult to be removed after hot rolling, and the coarsened ferrite caused expansion stress in the two phases, at which microcracks appeared when the expansion stress was greater than the strength limit of the steel. The ferrite content was calculated by the area algorithm. As shown in Fig. 9c, the ferrite content exhibited a downward trend with the addition of copper. The ferrite content decreased sharply at high pre-rolling temperature.

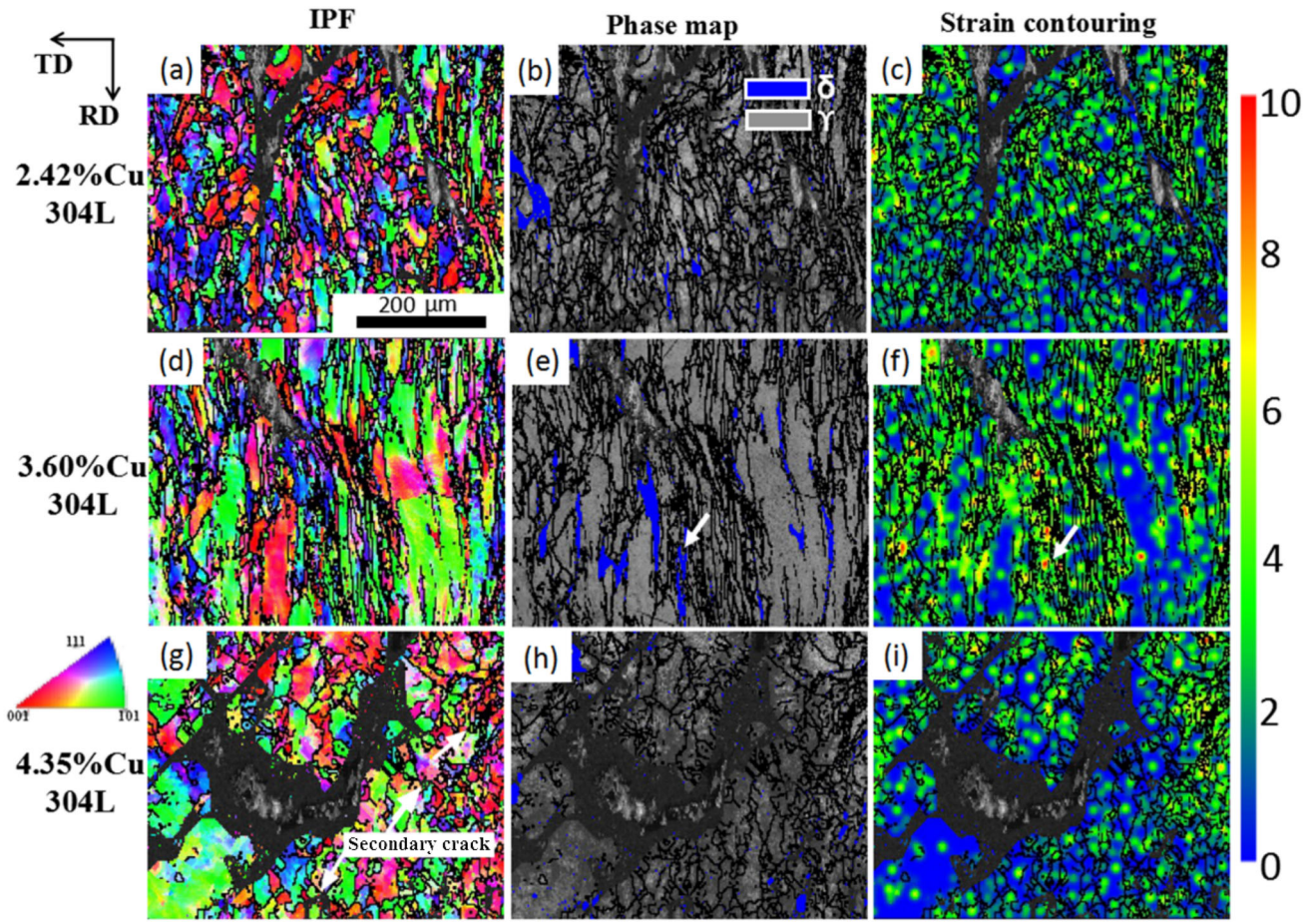

Fig. 8 IPFs, phase maps and strain contouring of microstructure around crack tip at 1250 °C. **a–c** 2.42%Cu 304L steel; **d–f** 3.60%Cu 304L steel; **g–i** 4.35%Cu 304L steel

Table 3 Solidification mode of austenitic stainless steel with different copper contents

Steel	304L	2.42%Cu 304L	3.60%Cu 304L	4.35%Cu 304L
Cr_{eq}/Ni_{eq}	1.95	1.61	1.44	1.34
Solidification modes	FA	FA	AF	AF

Chromium equivalent $Cr_{eq} = Cr + 1.4Mo + 1.5Si + 2Nb + 3Ti$; nickel equivalent $Ni_{eq} = Ni + 0.31Mn + 22C + Cu + 14.2N$

The study of Xu et al. [19] shows that in the as-cast or forged steel, the ferrite content between 15% and 30% will maintain good toughness with the matrix. It is shown in Fig. 6 that the cracks were distributed along the ferrite bands, and the ends of the cracks were connected with ferrite. The strain diagrams in Figs. 7 and 8 clearly show that the value of strain around ferrite was high, indicating the stress concentration at this place. TEM shows the detailed microstructure of the steel in the two-phase region as shown in Fig. 10. A high concentration of dislocations near the austenite/ferrite interface led to the inhomogeneity of the two-phase deformation. Ferrite, as a soft phase, preferentially undergoes large plastic deformation. With the increase in rolling force, the damage accumulation in ferrite and the incompatibility of plastic deformation between ferrite and austenite brought about voids as well as crack initiation and propagation at the austenite/ferrite interface [20, 21]. However, Liu et al. [22] reported that fine and slender ferrite formed between the banded grains after rolling. When the local maximum strain around the ferrite decreased, the maximum stress of some ferrite tip attachment decreases correspondingly, and the maximum stress of some tip attachments of ferrite decreased, helping to inhibit the generation of cracks. In addition, the banded structure had an effect on the austenite stability in steel [23]. The mechanical stability of austenite could be improved by promoting the uniform distribution of stress and strain.

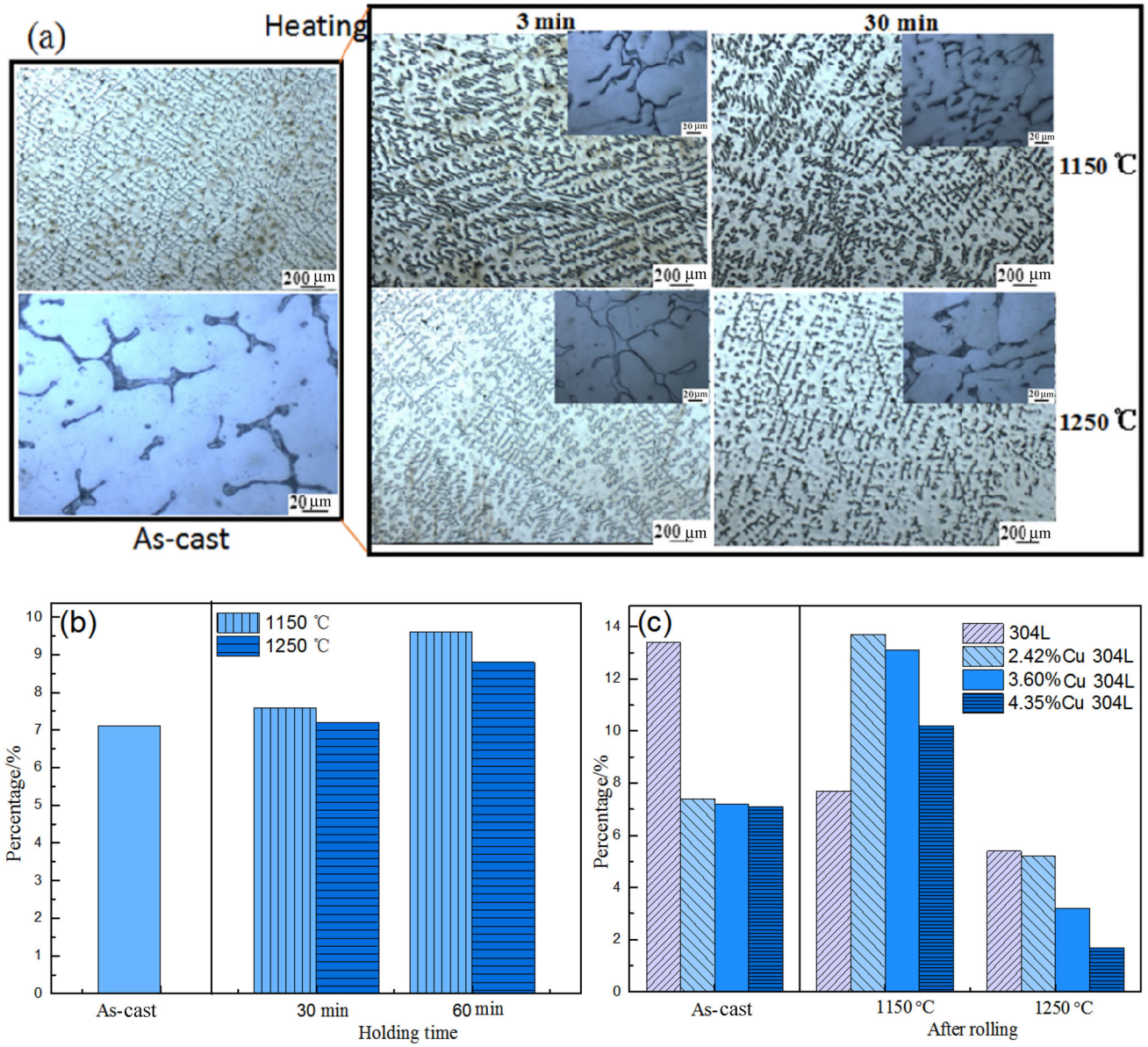

Fig. 9 Comparison of ferrite content of copper-containing austenitic stainless steel in different states. **a** 4.35%Cu 304L steel ferrite shape in as-cast heated states; **b** ferrite percentage in 4.35%Cu 304L steels in as-cast and heated states; **c** ferrite percentage of austenitic stainless steel with different copper contents

4.2 Effect of copper on hot working process

As can be seen from phase maps of Fe–Cu binary alloy calculated by Thermal-Calc software, Fe and Cu co-existed in the form of solid solution. Moreover, the melting point of copper (1084.5 °C) was far lower than the rolling temperature, and the copper content in antibacterial stainless steel far exceeded the hot brittleness threshold of 0.35%, indicating that copper which had higher solid solubility than the matrix gathered together and existed as liquid copper during the heat preservation process. There were bright Cu and Ni elements at the interface between the stainless steel and the scale, as shown in Fig. 11a. Cu elements segregated at the grain boundaries and thus formed a solid Cu–Ni-enriched layer with Ni elements which had a high concentration in 304L steel. In the subsequent hot rolling process, the difference between the lattice distortion of the solute atoms in the grain and the grain boundary provided the driving force for the segregation at the grain boundary, making low-melting copper elements or impurities more likely to segregate at the grain boundary than in the grain (Fig. 11b–d). At the same time, the distortion energy of copper and iron both in the grain and at the grain boundary was different because the copper

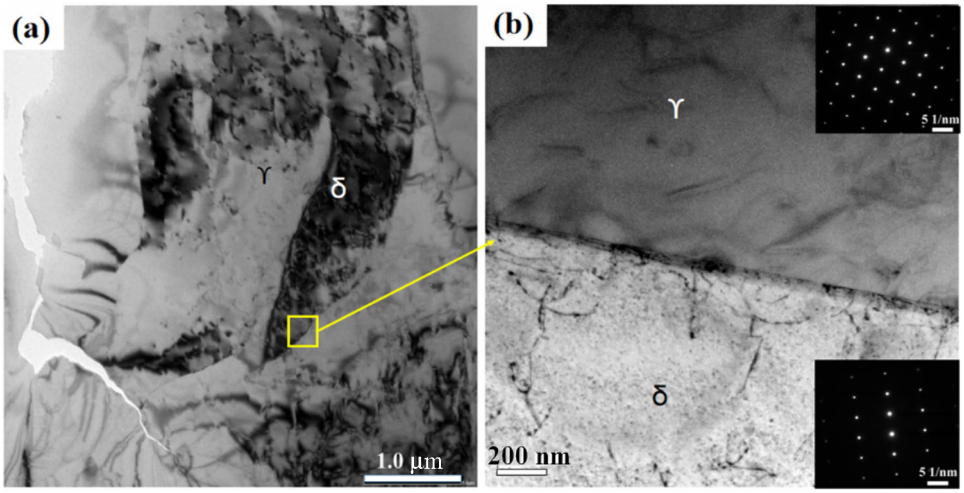

Fig. 10 TEM morphology of 4.35%Cu 304L steel. **a** TEM bright field image of ferrite in austenitic steel; **b** dislocation distribution near interface between austenite and ferrite in TEM enlarged structure

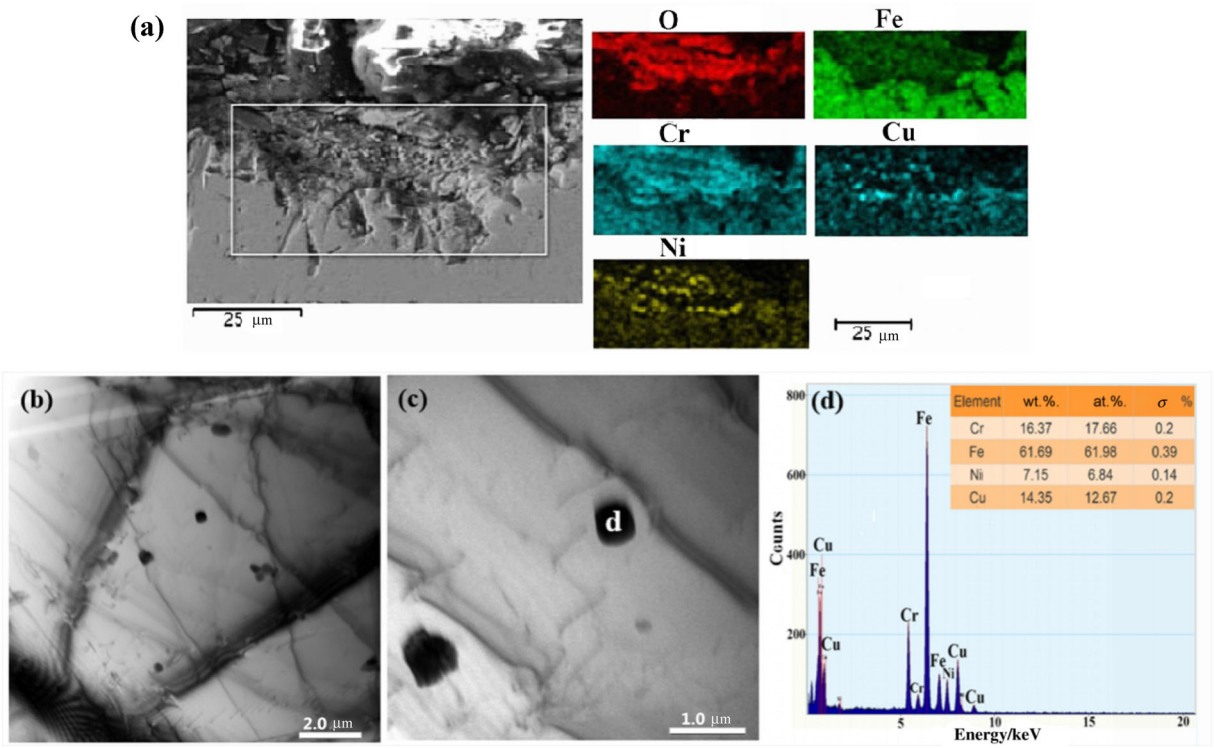

Fig. 11 Microstructure of 3.60%Cu 304L steel. **a** SEM and EDS of oxide layer on longitudinal section during heating; **b**, **c** TEM morphology of steel; **d** TEM–EDS of copper-rich phase

atoms had larger radius than iron atoms. In order to reduce the energy of the system, copper atoms preferentially segregated and precipitated at the grain boundary, which caused stress concentration. When the stress concentration reached the theoretical fracture strength, the copper elements diffused along the grain boundary reduced the strength of the matrix and led to the generation of cracks.

Both sides of the rolled plates spread in the rolling process. An additional tensile stress was produced at the edge due to the influence of the overall extensional fluidity of the metal, causing edge cracking of the plate [24]. A large number of dislocation tangles appeared in the grain during hot deformation. According to Eq. (1) [25], which represents the relationship between deformation and

dislocation density, the dislocation increased with the increase in deformation.

$$\rho = k^2\varepsilon^{2n}/(4b^2G^2\alpha^2) \quad (1)$$

where ρ is dislocation density; ε is true strain; n is deformation strengthening index; b is burgess vector; G is shear modulus of elasticity; k is the material constant; and α is scale coefficient of 0.5. A large number of dislocations formed around the copper element, and they acted as a good dislocation pipeline for the diffusion of copper, thus promoting the precipitation of copper (Fig. 11c). Meanwhile, the copper-rich phase and carbides accumulated dislocations, causing stress concentration, crack initiation and deepening of longitudinal cracks in the plate.

If the final rolling temperature is lower than the austenite recrystallization temperature during hot rolling, the austenite with seriously deformed structure mainly has two deformation textures: {110}<112> brass, and {112}<111> copper textures [26]. If the final rolling temperature is above the austenite recrystallization temperature, recrystallization occurs after hot rolling, and the {100}<001> cube texture component is enhanced. At 1150 °C, with the increase in copper content, the texture content of brass decreased from 26.8% to 22.5%, the content of copper texture increased from 22.1% to 30.8%, and the content of cube texture remained as lower as about 3% (Fig. 12). At 1250 °C, the content of brass and copper textures decreased with the increase in copper content, and the decrease was the most obvious when the content of copper was 4.35%. Especially, the copper texture content decreased the most, to only 0.5%. As a whole, the texture changes of 2.42%Cu 304L and 3.60%Cu 304L steel were small, while that of 4.35%Cu 304L steel was most obvious. The reason for different texture changes might be that the precipitated solid solution copper elements in austenite

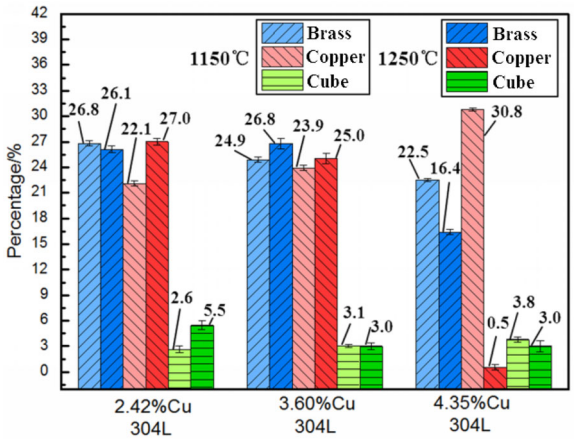

Fig. 12 Statistics of texture changes of austenitic stainless steel with different copper contents before rolling obtained from EBSD data at 1150 and 1250 °C

with the increase in copper content in the rolling process restrained partial recrystallization and affected the movement of sliding system, resulting in the change of texture orientation. The stacking fault energy of the copper-containing austenitic stainless steel, γ_{SFE}, was calculated by Eq. (2) proposed by Lu [27].

$$\gamma_{SFE} = -53 + 6.2x_{Ni} + 0.7x_{Cr} + 3.2x_{Mn} + 9.3x_{Mo} \quad (2)$$

where x_i stands for the content of element i.

With the addition in copper, the stacking fault energy of austenitic steel decreased slightly from 18.91 to 18.88 mJ/m^2, and the machinability of austenitic steel deteriorated. The previous study revealed that Cu segregated at dislocations and grain boundaries, which reduced the driving force of softening copper-containing 304L under the same deformation conditions, and hindered the continuous dynamic recrystallization process [28].

4.3 Cracking model

The cracking mechanism of 304L with different copper content at different pre-rolling temperatures is shown in Fig. 13. In the as-cast condition, the ferrite was distributed along the grain boundary of the steel. As the copper content increased, the ferrite volume increased and the ferrite content decreased (Fig. 9). Ferrite coarsened during heating, and it was distributed along the grain boundary and decreased with the increase in copper content after hot rolling. Meanwhile, the coarse grains elongated along the rolling direction, and the width of banded grains decreased with the increase in copper content. The chain-like recrystallized grains grew along the grain boundary as the temperature rose, but copper inhibited partial recrystallization, resulting in reduced recrystallization fraction. Some copper elements at the edge of the plate were dissolved in the steel in the heating process, especially around the ferrite. The further increase in the hot rolling reduction made the strain of ferrite larger, resulting in void formation and crack initiation and propagation at the austenite/ferrite interface. High copper content promoted the crack formation and propagation into the plate. The formation of surface cracks was very sensitive to temperature. Within the temperature range of 1100–1150 °C, the increase in temperature could inhibit the generation of surface cracks.

The increased temperature activated the potential slip system of the material, leading to the enhanced dynamic recrystallization and deformation ability and reduced deformation resistance. Meanwhile, a temperature difference of 50 °C between the center and the edge of the plate existed during the rolling process [29], which was larger at 1150 °C. Raising the temperature appropriately could improve the cracking resistance of the plate edge. Moreover, the iron-copper binary equilibrium phase

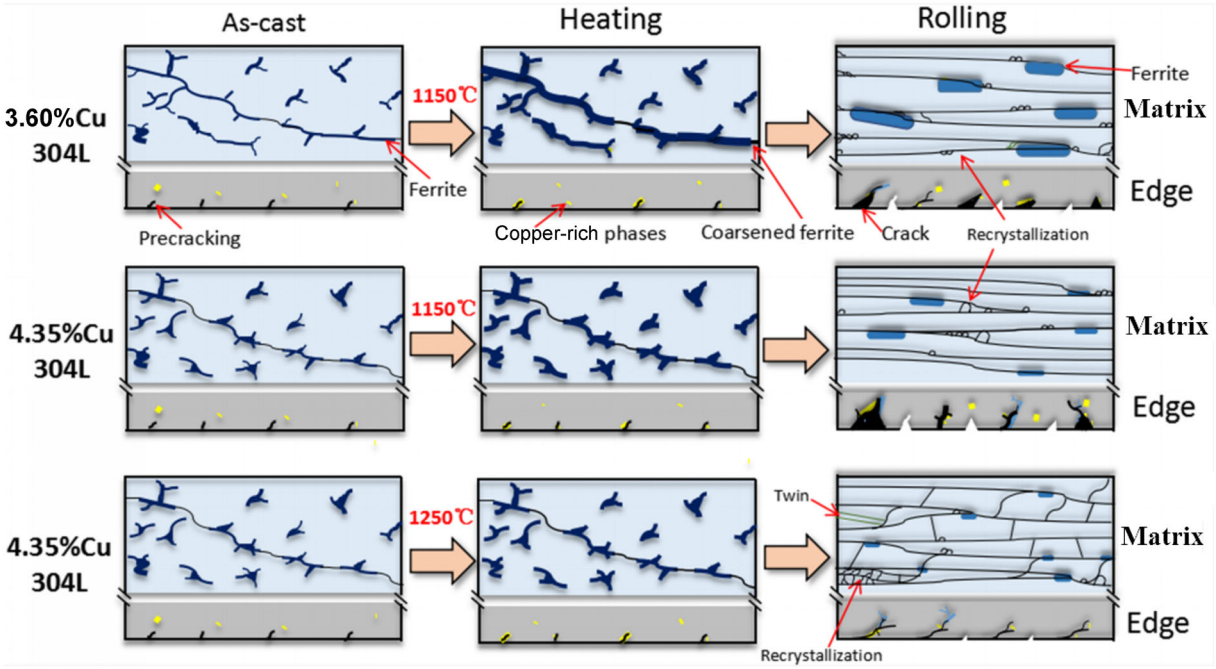

Fig. 13 Cracking mechanism of 304L with different copper contents at different pre-rolling temperatures

diagram suggested that the increasing temperature was helpful to improve the solubility of copper in steel and reduce the number of precipitated phases, thereby reducing the occurrence of cracks.

Therefore, in order to reduce the edge cracks, it is necessary to reduce the proportion of ferrite first and reduce the nucleation and propagation of cracks at the interface of two phases. It has been reported that the optimum conditions for the dissolution of ferrite could be determined by the highest rolling temperature and strain at thermomechanical treatment [30]. Secondly, it is also important to strictly control the copper content, deformation temperature, deformation rate, deformation amount and oxidation time in the process of deformation. Zhang and Wang [31] studied that adding Ni element to copper-containing steel can form copper nickel enrichment layer on its surface, increase compound melting point, avoid copper brittleness defect and reduce ferrite ratio. However, the addition of alloying elements will increase the material cost. Secondly, high temperature rapid combustion method can be used in industry at present [32]. At the same time, shortening the residence time from 1100 to 1150 °C and maintaining neutral or reducing atmosphere can effectively improve the edge cracking of plate. Thirdly, a continuous and stable Al_2O_3 anti-oxidation protective agent was sprayed or brush plated on the surface of antibacterial stainless steel before high temperature heating. It can prevent object oxidation, reduce the loss of high-temperature oxidation environment, and save the production cost of enterprises [33].

In a word, the addition of alloy content, the control of hot deformation conditions or high temperature oxidation resistant coating can effectively reduce the germination and propagation of surface cracks of copper-containing stainless steel, which has important research significance.

5 Conclusions

1. The increased copper content leads to the decrease in the width of banded grains along rolling direction after rolling at 1150 °C. The grain width increases with the rising temperature. The increase in copper content inhibits partial recrystallization and changes the texture orientation simultaneously.
2. The increase in copper content deteriorates the edge cracking of the plate, especially at 1150 °C. The crack gradually becomes deeper and its distribution is more continuous. The crack forms an angle of about 45° with the rolling direction, and extends from the side to the middle by about 14 mm maximally. The crack gets shorter and the crack depth becomes smaller as the temperature increases. Therefore, the pre-rolling temperature should be strictly controlled above 1150 °C in the heating process. Generally, the texture changes of 2.42%Cu 304L and 3.60%Cu 304L steels are small, while 4.35%Cu 304L steel texture changes considerably.
3. With the increase in copper content at 1250 °C, the content of {110}<112> brass and {112}<111> copper textures decreased. When the content of {112}<111>

copper was 4.35%, the decrease was most significant, and {112}<111> copper texture content decreased to only 0.5%. Generally, the textures of 2.42%Cu steel and 3.60%Cu steel changed little, while a large change in the texture of 4.35%Cu steel was observed. To conclude, the increase in rolling temperature can prevent edge crack and its propagation effectively.

4. The crack propagates along the ferrite and there are a lot of angular copper oxides. The main crack grows bigger with the increase in copper content. Oxidation occurs inside the cracks and the copper elements segregate during the hot rolling process, which accelerates the separation from the matrix interface. A large number of fine recrystallized grains form around the secondary crack, which effectively hinders the further extension of the crack.

Acknowledgements The project was supported by the National Key Research and Development Program of China (2016YFB0300205), Taiyuan University of Science and Technology Postdoctoral Research Startup Fund (20192024), Natural Science Foundation of Liaoning Province (No. 2019-KF-25-05), the Shanxi Province Science Foundation for Youths (201801D221120), the Key Research and Development Program of Shanxi Province (201703D111003), the Taiyuan University of Science and Technology Scientific Research Initial Funding (20172014), Shanxi Outstanding Doctorate Award Funding Fund (20182061), and the Coordinative Innovation Center of Taiyuan Heavy Machinery Equipment.

References

[1] L. Chen, R.B. Song, F.Q. Yang, Y.J. Wang, Z.D. Tan, K. Guo, Z.H. Wang, Mater. Sci. Forum 850 (2016) 66–71.
[2] K.K. Alaneme, S.M. Hong, I. Sen, E. Fleury, U. Ramamurty, Mater. Sci. Eng. A 527 (2010) 4600–4604.
[3] F.F. Luo, Z.H. Tang, S.F. Xiao, Y.L. Xiang, Mater. Technol. 34 (2019) 525–533.
[4] B. Prabha, P. Sundaramoorthy, S. Suresh, S. Manimozhi, B. Ravishankar, J. Mater. Eng. Perform. 18 (2009) 1294–1299.
[5] S.P. Tan, Z.H. Wang, S.C. Cheng, Z.D. Liu, J.C. Han, W.T. Fu, J. Iron Steel Res. Int. 17 (2010) No. 5, 63–68.
[6] N. Li, Journal of Liaoning University of Science and Technology 2 (2011) 157–162.
[7] T. Xi, M.B. Shahzad, D. Xu, Z.Q. Sun, J.L. Zhao, C.G. Yang, M. Qi, K. Yang, Mater. Sci. Eng. C 71 (2017) 1079–1085.
[8] H.Y. Fan, S.F. Liu, C. Deng, X.D. Wu, Q. Liu, Int. J. Refract. Met. Hard Mater. 72 (2018) 244–252.
[9] X.F. He, S. Wu, L.X. Jia, D.J. Wang, Y.K. Dou, W. Yang, Energy Procedia 127 (2017) 377–386.
[10] X.C. Li, J. Liu, W.X. Zhu, Y.C. Tang, X.L. Wang, Adv. Mater. Res. 1049–1050 (2014) 27–30.
[11] D. Ponge, G. Gottstein, Acta Mater. 46 (1998) 69–80.
[12] Y.M. Huang, C.X. Pan, Journal of Chinese Electron Microscopy Society 29 (2010) 662–672.
[13] C.X. Yue, S.J. Wu, L. Cao, H.L. Li, Forging and Stamping Technology 39 (2014) No. 11, 107–112.
[14] N. Suutala, Metall. Trans. A 14 (1983) 191–197.
[15] H.S. Bao, S.P. Tan, S.C. Cheng, Z.D. Liu, J. Iron Steel Res. 22 (2010) No. 2, 28–33.
[16] D. Li, Y.A. Min, X.C. Wu, J. Iron Steel Res. Int. 17 (2010) No. 11, 62–66.
[17] S.H. Kim, H.K. Moon, T. Kang, C.S. Lee, Mater. Sci. Eng. A 356 (2003) 390–398.
[18] Y. Wang, W.Z. Shao, L. Zhen, L. Lin, X.M. Zhang, Key Eng. Mater. 353–358 (2007) 515–518.
[19] Y.D. Xu, F. Han, T. Han, Z.J. Zhang, Hot Working Technology 44 (2015) No. 8, 94–96.
[20] H. Ghadbeigi, C. Pinna, S. Celotto, J.R. Yates, Mater. Sci. Eng. A 527 (2010) 5026–5032.
[21] N. Haghdadi, P. Cizek, P.D. Hodgson, V. Tari, G.S. Rohrer, H. Beladi, Acta Mater. 145 (2018) 196–209.
[22] M.X. Liu, Y.Q. Li, Z.S. Cui, Q. Yang, Mater. Charact. 156 (2019) 109828.
[23] B.L. Ennis, C. Bos, M.P. Aarnts, P.D. Lee, E. Jimenez-Melero, Mater. Sci. Eng. A 713 (2018) 278–286.
[24] Y.J. Dong , L.Q. Wei , B. Fu, B.Z. Tao, Special Steel 39 (2018) No. 1, 13–17.
[25] J.D. L'ecuyer, G. L'espérance, Acta Metall. 37 (1989) 1023–1031.
[26] A. Kurc-Lisiecka, W. Ozgowicz, W. Ratuszek, J. Kowalska, Solid State Phenom. 203–204 (2013) 105–110.
[27] S. Lu, Q.M. Hu, B. Johansson, L. Vitos, Acta Mater. 59 (2011) 5728–5734.
[28] J. Li, G.H. Zhao, L.F. Ma, H.Q. Chen, H.Y. Li, Q.X. Huang, J. Mater. Eng. Perform. 27 (2018) 1847–1853.
[29] L.F. Ma, Z.N. Pang, Z.Y. Ma, H.J. Xu, Y.P. Jiang, Mater. Sci. Eng. 32 (2014) 665–670.
[30] M. Rezayat, H. Mirzadeh, M. Namdar, M.H. Parsa, Metall. Mater. Trans. A 47 (2016) 641–648.
[31] X. Zhang, C.J. Wang, Tianjin Metallurgy 2016 (2016) No. 4, 11–13.
[32] X.C. Huang, H. Zhang, Y.Z. He, Hot Working Technol. 39 (2010) No. 22, 42–44.
[33] C. Sun, X. Yang, Y.H. Wen, Journal of Chinese Society for Corrosion and Protection 37 (2017) 590–596.